Vibrational Modes and the Dynamic Solvent Effect in Electron and Proton Transfer

Paul F. Barbara,* Gilbert C. Walker, Terrance P. Smith

This article primarily reviews recent work on ultrafast experiments on excited state intramolecular electron and proton transfer, with an emphasis on experiments on chemical systems that have been analyzed theoretically. In particular, those systems that have been quantitatively characterized by static spectroscopy, which provides detailed information about the reaction potential energy surface and about other parameters that are necessary to make a direct comparison to theoretical predictions, are described.

Critically important examples of thermal charge-transfer processes in condensed phases are found throughout chemistry, biology, and materials science. The kinetics of specific charge-transfer processes dictate the efficiency of key photosynthetic and energy conversion systems, both natural and synthetic. Charge-transfer processes play a central role in other practical areas, such as energy storage, nonlinear optics, and the photostability of media exposed to high-intensity optical irradiation. From a fundamental standpoint, the study of charge-transfer processes, and in particular homogeneous electron transfer in solution, is at the forefront of the revolution in the molecular level understanding of chemical reactions in liquids.

The last decade has brought progress to many central problems in charge-transfer research, such as the role of the solvent, the involvement of vibrational degrees of freedom, the role of solute and solvent nuclear tunneling of the solvent and solute and related quantum mechanical effects, the pathway and "mechanism" of electronic interactions, including long-range electron transfer, and other aspects of biological and heterogeneous electron transfer. Much of this work has been made possible by the proliferation of new spectroscopies, such as time-resolved Raman spectroscopy and femtosecond spectroscopy. Major theoretical advances have included the development of new theoretical frameworks as well as the use of supercomputers in the simulation of molecular aspects of the solvent in charge-transfer processes and in the modeling of donor-acceptor interactions in complex organometallic systems and macromolecules, including photosynthetic systems.

In order to set the stage for a discussion of new ultrafast experiments on electron transfer (*1*) and proton transfer (*2*), it is useful to review briefly a few of the central principles in contemporary charge-transfer research. Excellent reviews of the foundations of electron-transfer theories, including results up to 1985, have been given by Newton and Sutin (*3*) and Marcus and Sutin (*4*). The discussion below emphasizes electron transfer, but in many respects it also applies to proton transfer. Most theories of electron-transfer reactions in solution are formulated in terms of a model in which the transferring electron is localized at a donor molecular site in the reactant and at a different acceptor molecular site in the product. The nuclear modes of the reacting solute and the solvent are represented by a set of harmonic modes. The intramolecular modes are typically assumed to have identical frequencies in the reactant and product. The complex degrees of freedom are typically modeled within linear response theory by a solvent coordinate. In the last few years, molecular dynamics calculations have been used to test the validity of linear response theory for electron-transfer reactions, and the results generally support the accuracy of this approximation (*5–7*).

The usual curves for an electron-transfer reaction with no nuclear degrees of freedom other than the solvent coordinate are shown in Fig. 1A. The strength of the coupling of the solvent coordinate to the electron transfer is quantified by λ, the nuclear reorganization energy (solvent reorganization energy, in this case). A central expression in electron-transfer theory, attributable to Marcus, is

$$\Delta G^{\ddagger} = \frac{(\lambda + \Delta G^{\circ})^2}{4\lambda} \qquad (1)$$

where $\Delta G^{\ddagger}$ is the activation energy for the electron-transfer reaction and ΔG° is the reaction free energy (driving force).

According to Eq. 1, as ΔG° is varied from a large positive value (endothermic electron transfer), the activation energy decreases until $\lambda = -\Delta G^{\circ}$, for which $\Delta G^{\ddagger}$ is zero and there is no barrier. As ΔG° is made more negative, $\Delta G^{\ddagger}$ increases and k_{et}, the electron-transfer rate, correspondingly decreases. This latter situation, denoted by the inverted regime, is portrayed in Fig. 1B. Many molecular examples exhibit the inverted regime. Closs and Miller have observed particularly well-defined experimental examples of the inverted regime kinetic effect (*8*) for an organic electron-transfer system.

In addition to the solvent coordinate, there are nuclear modes associated with intramolecular vibrational motion. Vibrational modes have been treated in electron-transfer theory classically, quantum mechanically, or both. An electron-transfer reaction in the inverted regime for a model system with a single high-frequency vibrational mode is portrayed in Fig. 1B. The vibrational levels correspond to excitations of a mode that is "orthogonal" to the low-frequency classical vibrational mode.

Although a number of alternative electron-transfer theories have been formulated, most make use of fluctuations of the classical degrees of freedom to induce the electron-transfer event (*1–4*). Electron transfer occurs most rapidly at the curve crossings (circled regions in Fig. 1C). For models with high-frequency modes, as depicted in Fig. 1C, there are multiple vibronic crossings. The effective coupling strength at each vibronic curve crossing is a product of two factors ($V_{eff} = V_{el}\chi$). The first, V_{el}, is the electronic coupling matrix element, which reflects the electronic interaction between the donor and acceptor sites. There has been enormous progress in the calculation of V_{el} for various types of electron-transfer reactions, as reviewed by Newton (*9*). The second factor, χ, is the vibrational overlap integral (Franck-Condon factor) for the specific channel. Poor vibronic overlap of the high-frequency modes of the solute slows down the electron-transfer process.

The kinetic impact of high-frequency vibrational modes in electron transfer was explored theoretically in detail in the late 1970s and early 1980s by Kestner, Jortner, Bixon, Dogonadze, Kuznetsov, Ulstrup, Newton, Fischer, and others, as reviewed by Newton and Sutin (*3*). These studies showed that high-frequency modes can be

P. F. Barbara and G. C. Walker are in the Department of Chemistry, University of Minnesota, Minneapolis, MN 55455. T. P. Smith is in the Graphic Research Laboratory of 3M, St. Paul, MN 55133.

*To whom correspondence should be addressed.

especially important in the inverted regime (Fig. 1C). In the inverted regime, these modes can accelerate k_{et} by many orders of magnitude because the various vibronic channels allow for curve crossing with much smaller activation energies than those allowed in a purely classical theory (*10*) (Fig. 1B). An interesting recent experimental observation of the predicted effect was made recently by Liang, Miller, and Closs (*11*). However, the theoretical picture we just reviewed is from the pre-1980 theory. It has been somewhat altered by more contemporary results that include

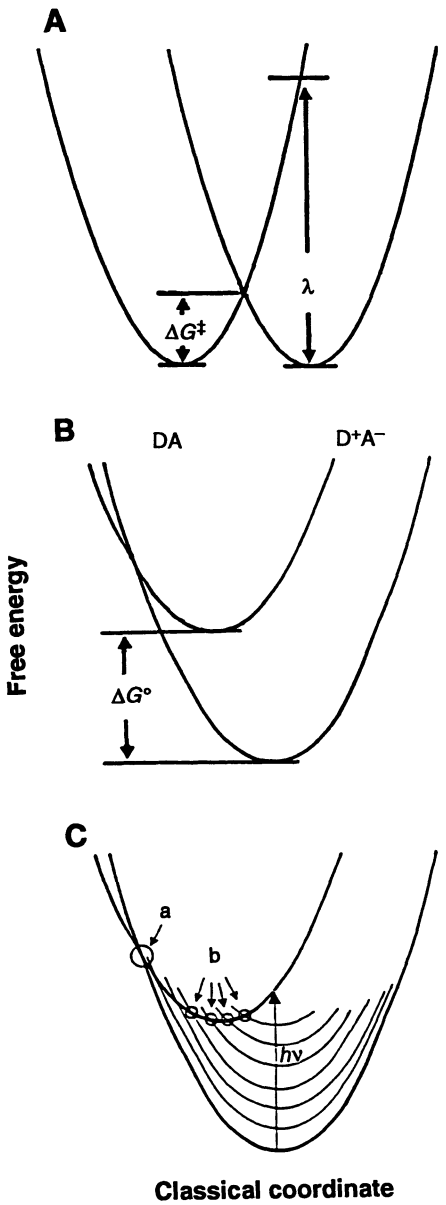

Fig. 1. Free-energy surfaces representing the localization of the transferring electron on the donor (DA) and the acceptor (D^+A^-). The classical reorganization energy is λ, the reaction free energy is $\Delta G°$, and the classical barrier to the reaction is $\Delta G^‡$. (**A**) $\Delta G° = 0$. (**B**) $\Delta G° + \lambda < 0$. (**C**) Same as (B), with the addition of a quantum vibrational mode in D^+A^-.

the role of solvation dynamics in electron-transfer kinetics, as discussed below.

One of the most interesting aspects of the basic formulation of thermal electron-transfer theory (Fig. 1) is its close relation to the Franck-Condon model for optical electronic transitions (or bands), which establishes a connection between spectroscopy and kinetics. Optical charge-transfer spectra can be used to determine many (and in some cases all) of the parameters required to predict k_{et} from thermal electron-transfer theory. The use of the integrated oscillator strength of a charge-transfer band to determine V_{el} was pioneered by Hush (*12*). Ulstrup and co-workers in particular have extensively developed charge-transfer band-shape analysis to determine effective vibrational and solvation parameters (*13*). For a recent interesting application of optical charge-transfer band analysis to electron transfer between radical pairs, see Gould *et al.* (*14*). Hupp and co-workers have established the use of resonance Raman spectroscopy of charge-transfer bands as a powerful tool to determine vibrational parameters for electron-transfer reactions (*15*).

Solvent Dynamics

A major focus of recent theoretical electron-transfer research has been the dynamic solvent effect, which is the kinetic consequence of noninstantaneous adjustment of the solvent coordinate and the solvent molecular orientation to the electron transfer, as discussed in recent reviews (*1, 16–21*). The qualitative result of this work is that, under certain conditions, k_{et} is predicted to be a function of the relaxation dynamics of the solvent, not just of the quasi-equilibrium solvent properties. For example, in models that ignore the effect of vibrational modes and use a simple description of solvation dynamics, k_{et} is predicted to be approximated by the relation

$$k_{et} = \frac{1}{\tau_s} \exp(\Delta G^‡/RT) \qquad (2)$$

where τ_s is the time scale for relaxation of the solvent coordinate.

Thus, within these models the electron-transfer process is controlled by solvation dynamics if there is no barrier. The dynamic solvent effect in electron transfer is due to dielectric friction, as opposed to the kind of friction that has been implicated in cis-trans isomerization, namely, collisional friction.

Many aspects of the dynamic solvent effect in electron transfer have been explored with analytical theory, including the consequence of multiple solvent relaxation times, molecular effects, electronic nonadiabatic behavior, inertial solvent modes, and vibrational modes. Much of this research is beyond the scope of this article, and the reader is referred to other reviews on this topic (*1, 16–22*).

The physical significance of τ_s continues to be an active area of research. A few qualitative comments are useful. Solvation dynamics have been measured by the transient Stokes shift method with ultrafast fluorescence spectroscopy on polar fluorescent probes. These measurements by Barbara, Fleming, Maroncelli, Simon, and others show that solvation dynamics occur on the picosecond to nanosecond time scale, depending on the temperature and solvent (*1, 17, 23–26*). The measured solvation time, τ_s, is close to τ_l, the longitudinal relaxation time predicted from continuum theory by using dielectric data on pure solvents. Values of τ_s and τ_l are now available for a broad range of solvents. For reasons discussed below, we call τ_s the time scale for relaxation of the "slow modes" of solvation. Molecular dynamics simulations predict that solvation dynamics should exhibit multiple relaxation time scales with significant relaxation components on the tens of femtosecond time scale; these components would not have been resolved by previous transient Stokes shift measurements (*7, 17, 23–27*). Very recently, however, Fleming and co-workers reported the first direct experimental evidence of femtosecond time scale solvation dynamics in acetonitrile (*28*). A qualitative interpretation of the molecular dynamics data assigns the shortest time scale solvation components to inertial motion, whereas the longer time scale processes are associated with large-amplitude solvent motion. A more detailed discussion can be found elsewhere (*24*).

During the 1980s a number of experimental observations were made of electron-transfer rates that are correlated with τ_s, and, as such, they have been interpreted as examples of dynamic solvent effects (*1, 16, 29–31*). This research represents the strongest experimental evidence for the dynamic solvent effect in electron transfer. Much of this work has involved photoinduced, excited state intramolecular electron-transfer reactions in aromatic molecules.

The earliest observations of dynamic solvent effects on excited state electron-transfer rates were made by Huppert and Kosower [in (*1*)]. Barbara and co-workers studied the intramolecular excited state electron transfer of 9,9′-bianthryl (*30, 31*). A band-shape analysis of the emission and absorption spectra of this system allowed these researchers to show that this reaction is nearly barrierless and involves a large electronic coupling V_{el} between the donor and acceptor groups (*32, 33*). As predicted

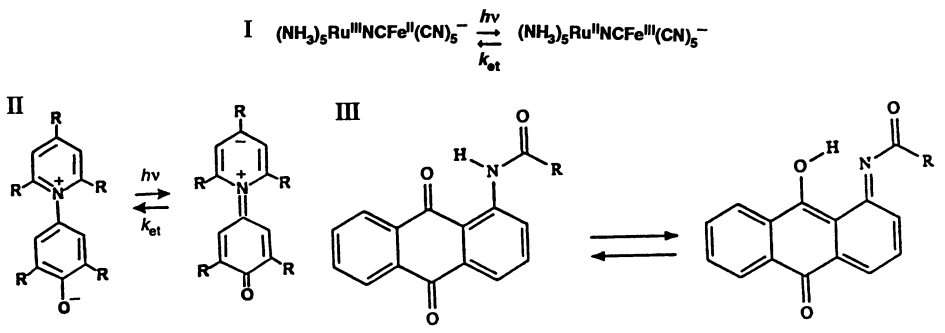

Fig. 2. Examples of charge-transfer reactions that have been studied in our laboratory. (I), A bridged, mixed valence, metal-metal electron-transfer reaction; (II), an intramolecular electron-transfer reaction; and (III), an intramolecular proton-transfer reaction.

by simple theory and simulation (*32*, *33*) for bianthryl, the observed electron-transfer rate k_{et} is approximately equal to τ_s^{-1} over a broad range of solvents and temperatures. Simon and co-workers also found evidence for correlations between k_{et} and τ_s^{-1} (*29*). However, these latter researchers observed that for the compound DMAPS the decay of the reactants' concentration is nonexponential and $k_{et} > \tau_s$. Both of these observations are inconsistent with simple theories of the dynamic solvent effect. The observations are in agreement, however, with the trends predicted by the theory of Sumi and Marcus (*34*), which combines solvation dynamics and vibrational promotion of electron transfer. This combined effect has also been dealt with and by Jortner and Bixon (*35*). The section below discusses these theories, and it reviews new experimental examples, from our laboratory, of molecules that involve vibrational effects in combination with the dynamic solvent effect (*36–39*).

Important experimental information on the dynamic solvent effect in electron transfer is available from the kinetic measurements of Weaver *et al.* on the thermally activated ($\Delta G^{\ddagger} \gg k_B T$), bimolecular, symmetric self-exchange reactions of metalocenes. There is strong experimental evidence that the rates of reactions in this class are correlated with τ_s^{-1}. For systems with extraordinarily small electronic matrix elements, however, Weaver *et al.* found that the electronic interaction between the donor and acceptor sites, rather than the solvation dynamics, is rate limiting (*16*).

Direct Optical Charge Transfer and the Dynamic Solvent Effect

Until very recently, most laser studies on intramolecular ultrafast electron transfer have involved conventional photoinduced intramolecular electron transfer, which can be represented as follows:

$$D\text{–}A\ (S_0) \xrightarrow{h\nu} D\text{–}A\ (S_1) \xrightarrow{k_{et}} D^+\text{–}A^-\ (S_1)$$

where D and A signify donor and acceptor groups (in many cases aromatic rings) and S_0 and S_1 denote the ground and the first excited electronic states.

Conventional photoinduced electron transfer has been of interest for decades. It is relevant to important processes such as photosynthesis and exciplex formation. From a fundamental standpoint, however, a complication is that little information may be available on the potential-energy surfaces of the reactant D – A (S_1) and product $D^+ - A^-$ (S_1) of these reactions. The situation is more favorable for direct photoinduced charge transfer from one site in a molecule to another.

$$(\text{Site 1, } e^-)(\text{Site 2}) \xrightarrow[k_{et}]{h\nu} (\text{Site 1})(\text{Site 2, } e^-)$$

Here an analysis can be made of the charge-transfer band shape to obtain various parameters of the potential energy surfaces of the reactant and product (as discussed above). The kinetics of the thermal electron-transfer process can be measured by transient absorption spectroscopy subsequent to "preparation" of the reactant by ultrashort laser excitation of the optical charge-transfer band.

We recently reported measurements on the kinetics of two important classes of direct photoinduced charge transfer (Fig. 2) (*36–40*). Reaction I involves a metal-metal intervalence charge transfer (MMCT) (*40*). Despite the fundamental importance of MMCT bands in many aspects of electron-transfer research, the kinetics of the thermal electron-transfer process after direct MMCT excitation had not been previously reported, although indirect measurements had been made by Creutz *et al.* (*41*). Only recently has the technology become available to measure the dynamics of MMCT with an adequate signal-to-noise ratio and sufficient time resolution.

Reaction II in Fig. 2 involves a class of organic compounds, the betaines, that have a charge-separated ground state (S_0) and a charge-recombined excited state (S_1). The thermal electron transfer is a charge-separation process. The enormous change in charge distribution upon optical excitation imparts a strong spectral sensitivity to environment. Indeed, the betaines are commonly used as spectroscopic solvent polarity probes (*42*). The dynamics of photoinduced charge transfer in betaines are discussed below (*36–39*).

Our experiments on the MMCT process have been limited to aqueous environments. In collaboration with Hupp, we have analyzed the MMCT transition, resonance Raman data on the MMCT band, and other information to determine effective potential parameters, such as $\Delta G°$ and V_{el} for the intervalence electron-transfer process. The thermal reaction is predicted to have a small $\Delta G^{\ddagger}$ and a relatively large V_{el}.

We have used three models to describe our experimental observations of the electron-transfer rate. The models include both solvation dynamics and vibrational modes but differ in their treatment of the vibrational degrees of freedom. Model A, a treatment by Sumi and Marcus (*34*), includes a low-frequency (classical) vibrational degree of freedom and a classical solvent degree of freedom. Model B, a treatment by Jortner and Bixon, (*35*) includes a high-frequency (quantal, $h\nu \gg k_{et}$) vibrational mode in addition to a classical solvent degree of freedom. Thus, model A involves a classical treatment of nuclear degrees of freedom, and model B involves a mixed classical-quantum description. Our model, model C, is a hybrid of models A and B that we developed recently by extending model A to include an additional high-frequency quantum vibrational mode. We show below that model C has the minimum nuclear degrees of freedom that are necessary to describe many electron-transfer reactions. These elements are (i) a solvent coordinate including dynamical effects, (ii) a characteristic high-frequency quantum mechanical vibrational mode of the reactant, and (iii) a low-frequency (classical) vibrational mode of the reactant.

Table 1 shows a comparison of predictions of the three models for Reaction I, with the spectroscopically determined potential energy parameters and the values of τ_s measured by the transient Stokes shift method. Considering the uncertainties in the experimental parameters and the simplicity of the models, the agreement between theory and experiment ($k_{et} \approx 10^{12}$ to $10^{13}\ s^{-1}$) is excellent. Thus, a direct test of these theories generally supports their validity.

A more in-depth analysis of the theoretical results reveals that all three models predict that this reaction is nearly barrierless and that solvation dynamics play an

Table 1. Predicted electron-transfer rates for $Ru^{II}Fe^{III} \rightarrow Ru^{III}Fe^{II}$, with associated parameters. The driving force $\Delta G^\circ = -4600$ cm^{-1}. The quantity Ω_{QM} is the frequency of the high-frequency, quantum mechanical accepting mode; $<\tau_s>$ is the average solvation time.

Theory	k_{et} (10^{12} s^{-1})	λ_{class} (cm^{-1})	λ_{sol} (cm^{-1})	$\lambda_{class,vib}$ (cm^{-1})	λ_{QM} (cm^{-1})	Ω_{QM} (cm^{-1})	$1/<\tau_s>$ (10^{12} s^{-1})
Model A	10 and 5*	5600	2400	3200		†	1.7
Model B	1.6	2400	2400		3200	1225	1.7
Model C	9	3250	2400	850	2400	1400	1.7

*Model A predicts two characteristic times for the electron-transfer process; see (*34*) and (*40*) for further details. †The average phonon frequency ν enters into model A ($\nu = 2.9 \times 10^{13}$ s^{-1}) as well as model C ($\nu = 8.5 \times 10^{12}$ s^{-1}). Model C for the betaines does not require the inclusion of ν.

important role. It is interesting that the models with high-frequency quantum modes (models B and C) give predicted rates similar to the classical only approach of model A. This situation should be contrasted to the strongly inverted regime electron-transfer reactions of the betaines, for which the predictions of the three models differ by many orders of magnitude, as discussed below.

In making the theoretical predictions we used a simple model in which the solvation dynamics are noninertial and characterized by a single relaxation time. The τ_s value of 0.6 ps from a transient Stokes shift measurement was used in the calculation (*1*). As discussed above, theory suggests that an additional inertial relaxation mechanism exists, with an effective relaxation time on the order of tens of femtoseconds. We ignore this type of solvation dynamics here because no experimental information on the amplitude and dynamics of this type of relaxation in the solvents we used is available. The impact of the inertial component of solvation dynamics is just beginning to be explored (*40*). McManis, Gochev, and Weaver (*43*) recently reported theoretical calculations indicating that the combined quantum effects of nuclear tunneling and electronic nonadiabaticity tend to mask the inertial effects on electron-transfer reactions in low-friction media.

We have made more extensive measurements on the betaines (*36–39*) than on MMCT complexes, which are more difficult to study in a range of solvents because of solubility limitations and poor spectral overlap with our ultrafast laser spectrometer. In contrast to electron transfer in MMCT reactions, betaine electron transfer occurs well within the inverted regime. For example, the potential energy as a function of vibrational modes, displacement of the solvent coordinate, and classical vibrations for betaine-30 in acetone is shown in Fig. 1C. The vibrational levels of an effective high-frequency mode are also shown. The parameters used to construct these curves come from fitting the observed optical charge-transfer absorption band shape. A comparison of experimental and theoretical k_{et} values for betaine-30 in the polar aprotic solvent glycerol triacetate (GTA) at various temperatures is shown in Fig. 3. The theoretical predictions were made by using the parameters from the band-shape analysis and τ_l (and alternative τ_s values) for the pure solvent.

The experimental rate is only weakly temperature-dependent. At low temperature, where the solvent responds at only a very slow rate, the observed k_{et} is much faster than $1/\tau_s$. This behavior should be contrasted to barrierless electron-transfer reactions such as the bianthryl case, where $k_{et} \approx 1/\tau_s$ over a large temperature range, including in slowly relaxing environments such as GTA. An extraordinary feature of the inverted regime electron transfer of the betaines allows this reaction to exceed the rate of solvation, as below.

A striking feature of the direct comparison to theory for the betaines is that the rates predicted from model A are too slow by more than six orders of magnitude. The primary cause of this discrepancy is the exclusively classical treatment of the vibrational coordinates that are used in model A. For inverted regime reactions the use of classical models for the vibrations tends to significantly overestimate the activation barrier because reaction occurs near the crossing of the purely classical surfaces for the reactant and product, that is, the region indicated by the bigger circle (a) in Fig. 1C. However, model B, which allows for electron transfer through vibronic channels [smaller circles (b) in Fig. 1C], gives a faster rate, in closer agreement with experiment, especially in solvents with τ_s values less than ~5 ps. Model B does fail, however, in slowly relaxing solvents because the only classical degree of freedom is the solvent coordinate, and the solvent coordinate cannot respond faster than τ_s.

Model C includes a classical intramolecular vibrational mode that is assumed to respond instantaneously and a classical solvent mode that responds according to τ_s. The predictions in Fig. 3 from model C have been made with no adjustable parameters; instead, only input from the band-shape analysis and the τ_s/τ_l details were used. The remarkable agreement between theory and experiment for model C is qualitative evidence that each and all of the elements listed in Table 1 are required for an accurate model of electron transfer in the inverted regime.

Further insight into the role of different nuclear degrees of freedom in the electron-transfer process can be gained by considering the dependence of τ_{et} (such as k_{et}^{-1}) on τ_s (Fig. 4). Most of the points in Fig. 4 represent different solvents at room temperature. The data points with $\tau_s \geq 12$ ps are all from GTA near room temperature. For

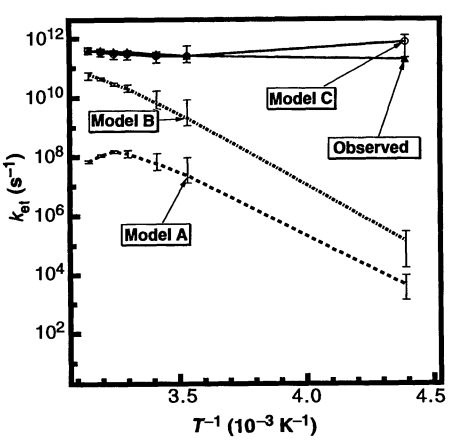

Fig. 3. Arrhenius plot for the electron-transfer rate of betaine-30 in GTA. The two lines near the top correspond to the experimental data and the predictions of model C. The middle line is the prediction of model B (by Jortner and Bixon), which includes quantum nuclear degrees of freedom of the solute but essentially has a rate limited by solvent dynamics. The lowest line is the prediction of model A (by Sumi and Marcus), which treats all nuclear degrees of freedom classically.

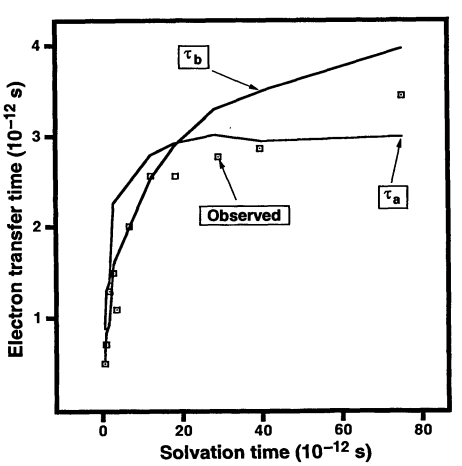

Fig. 4. The experimentally observed electron-transfer times (⊡) and the electron-transfer times (τ_a and τ_b) predicted by model C. For fast solvents, the predicted and observed times are a function of solvent dynamics. For slower solvents, intramolecular degrees of freedom control the electron-transfer rate.

small $\tau_s < \sim 3$ ps, τ_{et} varies almost linearly with τ_s, as is the case for barrierless reactions such as bianthryl electron transfer. In contrast, a much milder dependence on τ_s is seen for $\tau_s > 3$ ps. Theoretical predictions from model C are in good agreement with experiment over the entire τ_s range. The simulated results are expressed as τ_a, the average decay time of the reactant, and τ_b, the first moment of the decay kinetics of the reactant. For the theoretical estimates a separate, static charge-transfer spectrum was measured in each solvent, and potential parameters were obtained from the best-fit parameters of the model to the observed spectrum. For these calculations $V_{el} = 2500$ cm^{-1}, which was adjusted down slightly from the empirical value of 2900 cm^{-1} to improve agreement between theory and experiment by ~40% in all solvents. It should be emphasized, however, that this "adjustable parameter" is the same for all solvents.

The theoretical predictions of model C are in good agreement with experiment. A detailed analysis of the calculations provides insight into the physical effects that underlie the τ_{et} versus τ_s behavior. In order to develop this further, we need to examine briefly the physical nature of model C. The model is based on the electron-transfer theory of Sumi and Marcus (*34*), which is closely related to earlier, general approaches to frictional effects in chemical kinetics, such as the work of Bagchi and Fleming (*44*) and Agmon and Hopfield (*45*). In the Sumi-Marcus model the solvent coordinate is modeled classically and further assumed to evolve according to a diffusion equation with a diffusion constant that is inversely correlated with τ_s. The instantaneous probability distribution along the solvent coordinate is given by $P(X,t)$. The physical significance of $P(X,t)$ in DA can be seen in Fig. 5. In Fig. 5A the free energy is shown as a function of the solvent coordinate in the DA state, and Fig. 5B shows how $P(X,t)$ varies as a function of delay after laser excitation. If the reaction rate is strictly zero because $V_{el} = 0$—that is, no coupling occurs between DA and D^+A^-—then $P(X,t=0)$ reflects the equilibrium distribution of the ground state, which is "frozen" during the ultrashort excitation pulse. The probability $P(X,t)$ evolves with time because of the solvation process. The average value of X relaxes toward zero exponentially, with a relaxation time τ_s. The integral under $P(X)$ is called the survival probability $S(t)$ and reflects the fraction of reactant molecules surviving in the excited state at time t. Of course, if $V_{el} = 0$, no reaction occurs, and $S(t)$ does not decrease as time increases. However, when V_{el} is nonzero, the chemical reaction proceeds, and $P(X,t)$ and $S(t)$ reflect the evolving reaction.

In the Sumi-Marcus model, reaction occurs along the classical vibrational modes of the reactant with a solvent coordinate–dependent rate, $k(X)$. For example, if the solvent is frozen ($\tau_s = \infty$), the reaction occurs with a distribution of rates reflecting a distribution of solvent environments. Conversely, as τ_s approaches zero the solvent coordinate relaxes so rapidly that electron-transfer kinetics are similar to those of the pre-1980 models discussed above. As τ_s is varied from zero to infinity the rate in the Sumi-Marcus model tends to decrease, but under certain circumstances the trend would be more mild than $\tau_{et} \propto \tau_s$; that is, k_{et} would be faster than the evolution along the solvent coordinate.

Model C differs from the treatment of Sumi and Marcus in two ways. First, in our calculations we prepare the initial distribution, $P(X,t=0)$, as displaced along the solvent coordinate because the reaction is initiated by laser excitation of the ground state, which has an energy minimum that is displaced from the energy minimum of the excited state (Fig. 1C). Sumi and Marcus used an equilibrated solvent distribution at $t = 0$ in their simulations. The second difference is that they use an expression for $k(X)$ that includes multiple vibronic channels (Fig. 1C), whereas Sumi and Marcus used the Levich (*3*, *4*) expression for $k(X)$, which is a single vibronic channel (Fig. 1B) model, that is, a classical-only model for the vibrational degrees of freedom.

Figure 5C portrays log $k(X)$ for betaine in a typical solvent. Note that at values of X near where the system is prepared by laser excitation, $k(X)$ is much slower than at values of X near the minimum of the free-energy curve (Fig. 5A). The simulations reveal that in the slowly relaxing solvents ($\tau_s > 10$ ps) the evolution along X due to solvation is so slow that $P(X,t)$ decreases because of the reaction more rapidly than it shifts toward lower energy (Fig. 6A). The reaction is nearly at the frozen solvent limit, at which the predicted k_{et} is no longer dependent on τ_s.

In contrast, in quickly relaxing solvents ($\tau_s < 3$ ps) the transient solvation is so rapid that solvation occurs before reaction (Fig. 6B). In these environments, the decay of $S(t)$ and k_{et} is a function of τ_s. The complex interaction of solvation dynamics and electron-transfer kinetics causes the time dependence of the survival probability to be nonexponential. However, this subject is beyond the scope of this article.

In summary, the calculations from mod-

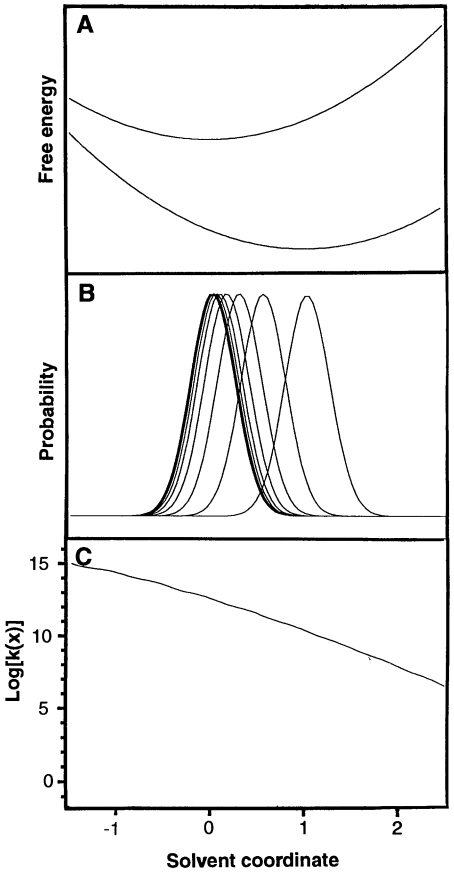

Fig. 5. (**A**) Free-energy surfaces generated with the potential parameters for betaine-30 in acetone. (**B**) Evolution of the probability distribution function, subject to the potential of the upper surface and the diffusion equation when $V_{el} = 0$. (**C**) Electron-transfer rate constant as a function of the solvent coordinate.

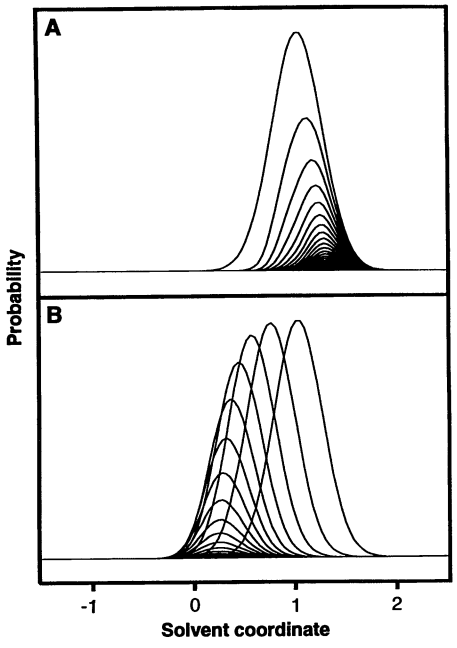

Fig. 6. Simulations of the probability distribution function for betaine-30 along the solvent coordinate at different times after photoinitiation in (**A**) a slowly relaxing environment (GTA, 293 K, τ_s = 125 ps) and (**B**) a quickly relaxing environment (acetone, 293 K, τ_s = 0.8 ps). The intervals between the plots are 1 ps in (A) and 0.25 ps in (B).

el C strongly suggest that the observed dependence of τ_{et} on τ_s can be assigned to two qualitatively different regimes: a solvation-controlled regime in which solvation dynamics is the rate-limiting process, and a frozen solvent regime in which the rate is controlled by thermal electron-transfer along vibrational coordinates. These two regimes are a natural consequence of the Sumi-Marcus model. It should be emphasized that in order to accurately describe ultrafast electron transfer in the inverted regime, it is necessary to modify the original Sumi-Marcus model by adding an additional high-frequency vibrational mode.

Another interesting feature of the electron-transfer kinetics of the betaines is the absence of a large activation energy. Similar behavior is observed for a broad range of fast electron-transfer reactions, including different electron-transfer steps in natural photosynthetic systems (*5, 17*). Model C predicts a very mild temperature dependence, with less than a factor of 3 decrease in rate from ambient temperature to 30 K if the potential parameters are fixed. In fact, the potential parameters do vary measurably (from the optical bandshape) over a large temperature range, and the prediction from model C deviates from the experimentally observed rate. This discrepancy, however, is much smaller than that for model A or model B.

Despite the predictive ability and transparency of the simpler electron-transfer models, such as models A through C, they are limited in several respects. First, these models use solvation dynamics that are overdamped and characterized by a single relaxation time. Recently, models that go beyond this approximation by including complex solvation dynamics with inertial effects have been developed by the use of molecular dynamics calculations and general quantum rate theory expressions, as seen, for example, in papers by Chandler (*7*), Hynes (*6*), Warshel (*5*), Schulten (*46*), and their co-workers.

A second problem with the simpler models is that they use a small number of effective vibrational modes (one or two) rather than a complete set of vibrational modes for the reactants. Because resonance Raman spectroscopy on charge-transfer bands gives detailed experimental information on multiple vibrational modes, it is possible in principle to make a multimode calculation of k_{et}. As mentioned above, quantum rate theory has recently made significant progress and may be a useful approach here. A related but distinct approach is the general Liouville space formalism for mixed quantum and classical systems (*22*). A stochastic, quantum mechanical Liouville equation (SLE) can be constructed and solved in principle for a general multimode system in the presence of a variety of media classes. The SLE can be viewed as being at the foundation of most electron-transfer theories (including models A, B, and C). Mukamel and co-workers have developed an approximate method of solving the SLE that is relatively inexpensive computationally and that is a promising approach for multimode electron-transfer systems. Jean, Fleming, and Friesner have applied multilevel Redfield theories to the multimode quantum rate process problem (analogous to electron transfer) by using extensive numerical simulation (*47*). These authors have observed that quantum coherences can have a dramatic effect. Coherences of this type are missing to varying extents in the simpler models. We have explored a phenomenological, strong adiabatic model for conventional photoinduced electron transfer and applied it to the interpretation of ultrafast emission data on 4-(9-anthryl)-*N,N'*-dimethylaniline (ADMA) and 9,9'-bianthryl (BA) (*33, 48, 49*). These results demonstrate that strong adiabatic effects can play an important role in ET when V_{el} is comparable to $\Delta G^{\ddagger}$.

Excited-State Intramolecular Proton Transfer

Excited-state intramolecular proton transfer has been extensively studied since the 1950s. A contemporary example from our laboratories is shown by reaction III in Fig. 2 (*50, 51*). Photoexcitation of the stable ground-state isomer (normal form) produces an electronically excited state of nitrogen that rapidly equilibrates with the excited state (tautomer form) by intramolecular proton transfer. As is the case of many other proton-transfer reactions, the rate of proton transfer k_{pt} is very rapid ($>10^{12}$ s^{-1}) in various environments, even at cryogenic temperatures. Other examples of molecules with extremely rapid intramolecular excited-state proton-transfer include 3-hydroxyflavone, hydroxybenzothiazole, 2-hydroxyphenylbenzothiazole, methylsalicylate, and other compounds (*2*). An unusual feature of reaction III is that the equilibrium constant can be varied over a large range by changing the solvent, the R group or both. This qualitatively establishes that the solvent coordinate is involved significantly in the proton-transfer reaction in polar solvents. However, $k_{pt} \gg \tau_s^{-1}$ in many cases, suggesting that a dynamic solvent effect is not observed for many reactions in this class, including reaction III.

Much less is known about the theoretical aspects of excited state ultrafast proton transfer than about electron-transfer reactions. Some researchers have used a Marcus-like model, where V_{el} of electron-transfer theory is replaced by the tunneling splitting Δ_{tun} due to quantum mechanical tunneling of the proton through a barrier within a double minimum potential, that is, the two tautomers (*2*). In this approach to modeling proton-transfer kinetics, the remaining nuclear degrees of freedom (solvent coordinate and vibrational modes) are modeled analogously to electron-transfer reactions. For recent examples, see the extension of this approach by Hynes and co-workers that allows vibrational modes to modulate Δ_{tun} (*52*) and the recent study by Voth and co-workers of different proton-transfer models (*53*) within the general thermal quantum rate processes theory of Voth, Chandler, and Miller (*54*).

Although there is too little information available on the potential energy parameters for excited state proton transfer to make a quantitative theoretical analysis, qualitative conclusions have been made. Frequency-resolved measurements on symmetric proton transfer molecules that are analogous to reaction III indicate that this reaction probably occurs by nuclear tunneling through a substantial barrier (*2*). The observation that the equilibrium constant is sensitive to the choice of solvent indicates that solvent motion is coupled to the proton-transfer process. However, the observation that $k_{et} \gg \tau_s^{-1}$ shows that vibrational modes promote the proton-transfer process (*50, 51*). Vibrational promotion of splitting of tunneling has been observed theoretically and experimentally in simpler systems (*2, 55, 56*). This is analogous to the behavior of the betaines in the more slowly relaxing solvents. Another closely related example is the excited state ($S_3 \rightarrow_{k_{et}} S_1$) intramolecular electron transfer of betaines (*39*). We have observed that this reaction proceeds at a rate that far exceeds τ_s^{-1} in all solvents; this reaction has been interpreted as having vibrationally controlled electron-transfer kinetics in all environments.

In contrast to the $k_{pt} \gg \tau_s^{-1}$ behavior of many other compounds (*2*), 3-hydroxyflavone in hydrogen-bonding solvents shows slow proton transfer that depends strongly on solvent and temperature (*57*). We have interpreted the kinetics of this system in terms of specific solute-solvent interactions. An alternative model for 3-hydroxyflavone in non–hydrogen-bonding solvents based on the dynamic solvent effect has been presented by Kelley and co-workers (*58*). Research on the dynamic solvent effect in proton transfer has just begun. We expect this area to expand rapidly in the near future.

REFERENCES AND NOTES

1. For recent detailed reviews on laser studies of excited-state electron transfer, see P. F. Barbara and W. Jarzeba, *Adv. Photochem.* **15**, 1 (1990); E.

M. Kosower and D. Huppert, *Annu. Rev. Phys. Chem.* **37**, 127 (1986).
2. Excited state proton transfer reactions are extensively discussed in the special issue *Chem. Phys.* **136** (no. 2) (1989) and in the review article P. F. Barbara, P. K. Walsh, L. E. Brus, *J. Phys. Chem.* **93**, 29 (1989).
3. M. D. Newton and N. Sutin, *Annu. Rev. Phys. Chem.* **35**, 437 (1984).
4. R. A. Marcus and N. Sutin, *Biochim. Biophys. Acta* **811**, 265 (1985).
5. A. Warshel and W. W. Parson, *Annu. Rev. Phys. Chem.* **42**, 279 (1991).
6. E. A. Carter and J. T. Hynes, *J. Phys. Chem.* **93**, 2184 (1989); D. A. Zichi, G. Ciccotti, J. T. Hynes, M. Ferrario, *ibid.*, p. 6261.
7. J. S. Bader and D. Chandler, *Chem. Phys. Lett.* **157**, 501 (1989); J. S. Bader, R. A. Kuharski, D. Chandler, *J. Chem. Phys.* **93**, 230 (1990).
8. G. L. Closs and J. R. Miller, *Science* **240**, 440 (1988).
9. M. D. Newton, *Chem. Rev.* **91**, 767 (1991).
10. M. Bixon and J. Jortner, *J. Phys. Chem.* **95**, 1941 (1991).
11. N. Liang, J. R. Miller, G. L. Closs, *J. Am. Chem. Soc.* **112**, 5355 (1990).
12. N. S. Hush, *Prog. Inorg. Chem.* **8**, 391 (1967).
13. E. M. Itskovitch, J. Ulstrup, M. A. Vorotyntsev, in *The Chemical Physics of Solvation, Part B*, R. R. Dogonadze, E. Kalman, A. A. Kornyshev, J. Ulstrup, Eds. (Elsevier, Amsterdam, 1986), chap. 6.
14. I. R. Gould, R. H. Young, R. E. Moody, S. Farid, *J. Phys. Chem.* **95**, 2068 (1991).
15. For example, see S. K. Doorn and J. T. Hupp, *J. Am. Chem. Soc.* **112**, 4999 (1990).
16. M. J. Weaver and G. E. McManis III, *Acc. Chem. Res.* **23**, 294 (1990); see references within to the work of Zusman, Cukier, and others.
17. M. Maroncelli, J. MacInnis, G. R. Fleming, *Science* **243**, 1674 (1989).
18. B. Bagchi, *Annu. Rev. Phys. Chem.* **40**, 115 (1989).
19. H. Frauenfelder and P. G. Wolynes, *Science* **229**, 337 (1985), and references within to earlier work by Wolynes.
20. B. B. Smith, H. J. Kim, J. T. Hynes, in *Condensed Matter Physics, Aspects of Electrochemistry*, M. P. Tosi and A. A. Kornychev, Eds. (World Scientific, New York, 1991), pp. 44–61.
21. I. Rips, J. Klafter, J. Jortner, *J. Phys. Chem.* **94**, 8557 (1990), and references within to earlier work from these and other authors.
22. S. Mukamel and Y. J. Yan, *Acc. Chem. Res.* **23**, 301 (1989).
23. J. D. Simon, *ibid.* **21**, 128 (1988).
24. M. Maroncelli, *J. Mol. Liq.*, in press.
25. W. Jarzeba, G. C. Walker, A. E. Johnson, P. F. Barbara, *Chem. Phys.* **152**, 57 (1991); W. Jarzeba, G. C. Walker, A. E. Johnson, M. A. Kahlow, P. F. Barbara, *J. Phys. Chem.* **92**, 7039 (1988).
26. M. A. Kahlow, W. Jarzeba, T. J. Kang, P. F. Barbara, *J. Chem. Phys.* **90**, 151 (1989).
27. T. Fonseca and B. M. Ladanyi, *J. Phys. Chem.* **93**, 230 (1991).
28. S. Rosenthal, X. Xie, M. Du, G. R. Fleming, *J. Chem. Phys.*, in press.
29. J. D. Simon and S. G. Su, *Chem. Phys.* **152**, 143 (1991), and references therein.
30. M. A. Kahlow, T. J. Kang, P. F. Barbara, *J. Phys. Chem.* **91**, 6452 (1987).
31. T. J. Kang *et al.*, *ibid.*, **92**, 6800 (1989).
32. T. J. Kang, W. Jarzeba, T. Fonseca, in *Perspectives in Photosynthesis*, J. Jortner and B. Pullman, Eds. (Kluwer Academic, Dordrecht, The Netherlands, 1989), pp. 273–292.
33. T. J. Kang, W. Jarzeba, P. F. Barbara, T. Fonseca, *Chem. Phys.* **149**, 81 (1990).
34. H. Sumi and R. A. Marcus, *J. Chem. Phys.* **84**, 4894 (1986).
35. J. Jortner and M. Bixon, *ibid.* **88**, 167 (1988).
36. E. Akesson, G. C. Walker, P. F. Barbara, *ibid.*, in press.
37. E. Akesson *et al.*, *ibid.*, in press.
38. G. C. Walker, E. Akesson, A. E. Johnson, N. E. Levinger, P. F. Barbara, *J. Phys. Chem.*, in press.
39. N. E. Levinger, A. E. Johnson, E. Akesson, G. C. Walker, P. F. Barbara, *Chem. Phys. Lett.*, in press.
40. G. C. Walker, P. F. Barbara, S. K. Doorn, Y. Dong, J. T. Hupp, *J. Phys. Chem.* **95**, 5712 (1991).
41. C. Creutz, P. Kroger, T. Matsubara, T. L. Netzel, N. Sutin, *J. Am. Chem. Soc.* **101**, 5442 (1979).
42. C. Reichardt, in *Molecular Interactions*, H. Ratajczak and W. J. Orville-Thomas, Eds. (Wiley, New York, 1982), vol. 3, pp. 241–282.
43. G. E. McManis, A. Gochev, M. J. Weaver, *Chem. Phys.* **152**, 107 (1991).
44. B. Bagchi and G. R. Fleming, *J. Phys. Chem.* **94**, 9 (1990).
45. N. Agmon and J. J. Hopfield, *J. Chem. Phys.* **78**, 6947 (1983).
46. M. Nonella and K. Schulten, *J. Phys. Chem.* **95**, 2059 (1991).
47. J. M. Jean, G. R. Fleming, R. A. Friesner, *Ber. Bunsenges. Phys. Chem.* **95**, 253 (1991).
48. K. Tominaga, G. C. Walker, T. J. Kang, P. F. Barbara, *J. Phys. Chem.* **95**, 10485 (1991).
49. K. Tominaga, G. C. Walker, W. Jarzeba, P. F. Barbara, *ibid.*, p. 10475.
50. T. P. Smith, K. Z. Zaklika, K. Thakur, P. F. Barbara, *J. Am. Chem. Soc.* **113**, 4035 (1991).
51. T. P. Smith *et al.*, *J. Phys. Chem.* **95**, 10465 (1991).
52. D. Borgis and J. T. Hynes, *J. Chem. Phys.* **94**, 3619 (1991).
53. D. Li and G. A. Voth, *J. Phys. Chem.*, in press.
54. G. A. Voth, D. Chandler, W. H. Miller, *J. Chem. Phys.* **91**, 7749 (1989).
55. N. Shida, P. F. Barbara, J. Almlöf, *ibid.* **92**, 4061 (1989).
56. ———, *ibid.* **94**, 3633 (1991).
57. A. J. G. Strandjord, D. E. Smith, P. F. Barbara, *J. Phys. Chem.* **89**, 2362 (1985).
58. G. A. Brucker and D. F. Kelley, *ibid.*, in press.
59. We acknowledge support by the Office of Naval Research and the NSF.

Energy Sources: A Realistic Outlook

Chauncey Starr, Milton F. Searl, Sy Alpert

Projections to the middle of the next century indicate that unabated historical global energy trends would lead to an annual global energy demand about four times present levels, primarily due to population and economic growth. But extensive global conservation and energy-efficient systems might reduce this value by half. The cumulative effect of the coming half century's use may strain the world's low-cost resources, particularly oil. The future fuel mix is further complicated by the environmental thrust to reduce the global use of carbon-based fuels. The interaction of the principal factors influencing future energy resource and technology options are projected.

The energy supply mix of the coming century will depend on the magnitude of the demand growth for global energy, changing performance targets, and the technologies available to meet them. Historically, major changes in fuel use patterns have resulted from new conversion and end-use technologies and from shifts induced by demand growth and by changed societal priorities and objectives. The development of new technologies has been crucial to such fuel use changes by providing the means and options for new performance targets. This article reviews the spectrum of future supply options and their flexibility for meeting the large global energy needs foreseen in the next century.

The future adequacy of globally available fossil fuel resources will depend on the total societal costs of extracting and delivering such fuels and on their effectiveness in use to meet the broad performance objectives of energy systems. Projections of proven, probable, and speculative resources are often updated as new discoveries or extraction techniques are developed, but professional conservatism has often resulted in underestimating future resource expansion at acceptable costs. On a next century time scale, the traditional question is whether the cumulative effect of the increasing rate of depletion of these resources would result in a global constraint on energy systems, particularly on the future supply of liquid fuel for vehicles and airplanes. This question is technologically intriguing because of the now demonstrated large-scale convertibility of all fossil fuels to gas or liquid forms and the implications of the application of this technology as an option for a global source of liquid fuel derived from large coal resources.

The present global energy mix is likely to change substantially during the next century as a result of several factors. First, comparative scarcity attributable either to resource or to political constraints may increase the relative price of the most convenient fossil fuel, oil; second, the growing costs of reducing environmental degradation will alter the cost competition among fuels; and third, the potential threat of global climate change may stimulate a shift from carbon-based fuels to nonfossil alternatives. A resource perspective for the next century involves speculation on future energy demand, likely competitive supply al-

The authors are at the Electric Power Research Institute, Palo Alto, CA 94303.